Hydro-mechanical numerical analysis of fault reactivation due petroleum production as trigger for submarine slope stability

Tasso Carvalho da Silva[1#] (ID), Igor Fernandes Gomes[1] (ID), Tiago Siqueira de Miranda[2] (ID),

Julliana de Paiva Valadares Fernandes[3] (ID), José Antônio Barbosa[4] (ID),

Leonardo José do Nascimento Guimarães[5] (ID)

Article

Abstract

Oil production in offshore regions involves the transportation of oil and gas in submarine pipelines, which are vulnerable to geological processes triggered by subsurface oil production like fault reactivation. The fault reactivation process can lead to phenomena that impact the seabed, like subsidence and fluid exudation, and can trigger instability of submarine slopes, which can result in environmental and economic damage. The present work addresses a coupled hydromechanical numerical modeling of a hypothetical case involving fault reactivation caused by oil reservoir production and its impact on an overlying submarine slope. The hypothetical case was simulated using a finite element model. The case involves a reservoir which is cut by a fault zone that reaches the seabed. The slope instability studied was induced by the injection and production of fluids in the reservoir. The fault zone is assumed to be a sealing region and a geomechanical and pressure field discontinuity within the reservoir. Int this work was used the Mohr-Coulomb elastoplastic model with Perzyna viscoplastic regularization to represent the behavior of the fault zone and the overlying submarine slope. Results showed that the fault reactivation, caused by the reservoir production, developed shear stress and shear plastic strain along the fault and through the submarine slope, causing horizontal and vertical displacements in the slope mass and acting as a trigger factor for slope stability. Pore pressure increase at the bottom of the slope structure correlated with the injection pressure artificially increased into the reservoir.

1. Introduction

The injection and production of fluids in oil and gas reservoirs can cause significant changes to the stress state of the rocks, resulting from changes in the pore pressure. Reservoir interventions can lead to the concentration of shear stresses in fault zones in the reservoir or nearby, and cause reactivation.

Geological faults form discontinuity regions and damage zones between blocks of rocks, and are characterized by the parallel movement of broken parts (Peacock et al., 2017). Faults are characterized by the parallel movement of the rupture surface, and the fault plane can be flat or curved. Faults with sealing capacities (very low permeability zones)

are important to forming hydrocarbon traps by preventing fluid migration through porous media. Fault zones consist of two main regions: a fault core, and a fault damage zone (Billi et al., 2003; Gudmundsson, 2004; Mitchell & Faulkner, 2009; Choi et al., 2016; Fossen, 2016; Celestino et al., 2020; Souza et al., 2022). Each region in a damage zone has specific shear strength and stiffness, porosity, permeability, and other properties heterogeneously distributed along its length and depth (Choi et al., 2016).

A damage zone is the network of subsidiary structures that involves the fault core and can increase the permeability of the fault zone in relation to the core and the undeformed protolith. Fault-related subsidiary structures in damage zones include small faults, veins, fractures, cleavages, and

Silva et al., Soil. Rocks, São Paulo, 2023 46(4):e2023006523

1

folds that contribute heterogeneity and anisotropy to the permeability structure and elastic properties of the fault zone (Matsumoto & Shigematsu, 2018). Large damage zones can indicate multiple slipping episodes and the overprinting of successive deformation events (Caine et al., 1996; Choi et al., 2016; Torabi et al., 2020).

Studies of fault zones show how properties differ significantly, depending on the region analyzed, from the fault core to the undamaged rock. Cappa & Rutqvist (2011) argue that the fault core is a region of low permeability with small intergranular porosity, while the damage zone is more permeable, but less permeable than the reservoir, as a result of its macroscopic fracture network.

Gudmundsson (2004) showed how the development of the fault core and the damage zone can affect the mechanical properties, in particular the Young's modulus, of the host rock. The author also demonstrated an example regarding the distribution of the elastic modulus (Young) across the fault zone, from the undamaged host rock to the fault core.

Myers (1999) studied a fault zone in an outcrop of the Aztec sandstone located in the Valley of Fire State Park, USA. The fault consists of five structural elements with distinct characteristic permeabilities. The damage zone is formed by joints, sheared joints, fault cores, and slip surfaces, which are embedded in the undisturbed host rock.

The fault reactivation process can be characterized by shear strains and loss of the sealing characteristic due to dilation, which is the increase in volume associated with the shear deformation. Several works have addressed the numerical hydro-mechanical modeling of fault reactivation problems, such as Khan et al. (2020), Quevedo et al. (2017), Yang et al. (2021), Rutqvist et al. (2007), Soltanzadeh & Hawkes (2008) and Guimarães et al. (2009, 2010).

Fault reactivation can lead to seabed deformation and exudation of fluids on the seabed surface. Interventions during reservoir production can affect geological faults and destabilize submarine slopes. Submarine slope instability can lead to landslides, and hence tsunami (Gue, 2012; Ma et al., 2013), damage to offshore pipelines (Zhang et al., 2019) and offshore wind towers (Bakhsh et al., 2021), and extensive environmental and economic damage.

There are few and important studies on the risks and effects of submarine slope instability, the failure, and effects like landslide as Masson et al. (2010), Gue (2012), Urgeles & Camerlenghi (2013), Katz et al. (2015) and Scarselli et al. (2016). Scarselli (2020) provided a general view of key factors related to submarine landslides such as classification schemes, architectural elements, preconditioning, and triggering factors. The author studied the causes of submarine slope failure and the environments of occurrence, finding trigger factors such as increased pore pressure due to fluid migration and seepage, and the slope steepening due to faulting, folding, and diapirism.

Yincan (2017) discussed several topics related to submarine landslide theme, like classification and instability

mechanisms and methods for analyzing stability. These authors treated statistical data of submarine slope instability events and their triggering factors like earthquake and fault activities, shallow gas or natural gas hydrate exudation, human activities, and erosion effects.

Various stability analysis methods for submarine slope have been commonly used, such as the limit equilibrium method, and analytical and numerical methods, as proposed by Leynaud et al. (2004), ten Brink et al. (2009), Quinn et al. (2011, 2012), Puzrin et al. (2015), Dey et al. (2016). Numerical analysis allows prediction of the stress state and displacement field for the slope structure and the surrounding structures below the submarine slope. This type of analysis adopts constitutive models, which allows the definition of the stress-strain inelastic (regarding a rate-dependent or independent plasticity) behavior. Finite element methods are commonly used to represent small-strain (Lagrangean) or large-strain (Eulerian) related mechanical phenomena (Dey et al., 2016; Stoecklin et al., 2021). Methods like the material point and the discrete element approach are also commonly used, especially for post-failure simulation. The analysis of total or effective stress of submarine slopes can be treated through numerical simulations with reliable results and it allows to reduce risks.

Overall, the study of fault reactivation impact on submarine slope stability scarcely regards the contexts of oil and gas production or CO_2 storage. The hypothesis of this work is that the geological faults and the related kinematics are impacted by the increase in pore pressure created by fluid flow along the fault structure, which can trigger fault reactivation and slope instability. The present work uses a novel approach to analyze a hypothetical case study on submarine slope stability, considering the scenario of a geological fault reactivation as the trigger. The scenario involves a shallow offshore reservoir production and a normal fault that cut the reservoir.

The study uses a coupled hydromechanical numerical simulation of fluid flow in the context of oil reservoir production with the possibility of fault reactivation. The simulation is able to demonstrate the impact of the fault reactivation process on the stress-strain response of a submarine slope above the reservoir, through the Mohr-Coulomb viscoplastic model, and viscous Perzyna regularization (Perzyna, 1966). The model is simplified by treating the fault zone and the core as a homogeneous, continuous medium. The simulation was carried out using in-house finite element code (Olivella et al., 1995; Guimarães et al., 2007; Silva et al., 2021; Souza et al., 2022), and a 2D finite strain analysis was considered. The post-failure slope behavior was not investigated here.

2. Mathematical modeling

Soils and rocks are complex porous media which need adequate constitutive models to describe each type of material. Thus, elastoplastic constitutive models are used to represent

2

Silva et al., Soil. Rocks, São Paulo, 2023 46(4):e2023006523

the elastic and plastic behavior as a response to stresses to which the material is submitted. The model describes the material strain in two parts, elastic vs plastic, and reversible vs irreversible. In this work, the hydro-mechanical simulation was formulated considering the governing equations for the mass and moment balance in each phase. The geomechanical problem presents the stress-strain behavior of the rock, which depends on the state of the stresses and the pore pressure field. For simulating the hydraulic effects, the permeability and porosity of the porous media are updated at each time step. Infinitesimal (small) strain effects, and constant-temperature equations were considered for the calculations, regarding the mechanical problem defined by the Cauchy equilibrium equation (Equation 1). This approach considered constitutive laws and complementary equations, and the hydraulic problem is characterized by the mass balance of the fluid phase using Darcy's law (Equation 2).

$$\nabla \sigma + b = 0 \qquad (1)$$

where ∇ is the divergence operation on the stress tensor σ, and b is the volumetric vector of the body forces. The phase mass balance is represented by:

$$\frac{\partial \phi \rho_l}{\partial t} + \nabla.\left(\rho_l q_l\right) + \rho_l \phi \nabla \dot{u} + f_l = 0 \qquad (2)$$

where ρ_l is the density of the fluid phase, ϕ is the porosity of the rock, q_l is the Darcy's flux vector, and f_l is a source/sink mass term of the fluid phase. The invariants of the problem are the nodal displacement vector $\dot{u}$, and the nodal fluid pressure p_l. The main constitutive equation for the hydraulic problem is Darcy's Law; in this work, only a single-phase fluid flow is considered:

$$q_l = \left(\frac{K}{\mu_l}\right)(\nabla p_l + \rho_l g) \qquad (3)$$

where K is the intrinsic permeability tensor of the porous medium, μ_l is the viscosity of the fluid phase, and g is the gravity vector.

2.1 ElastoViscoplastic constitutive model

It was adopted the Mohr-Coulomb elastoplastic model with viscous regularization by Perzyna's model (Perzyna, 1966; Simo & Hughes, 1998), where the stress and strain increments are described as follows:

$$d\sigma' = D^e d\varepsilon = D^e(d\varepsilon^e + d\varepsilon^{vp}) \qquad (4)$$

In which $d\sigma'$ is the effective stress increment, D^E is the elastic constitutive tensor and the variables $d\varepsilon$, $d\varepsilon^E$, $d\varepsilon^{VP}$ are, respectively: the increment of total, elastic and viscoplastic strains. The stress vector is determined by the effective stress principle, where the stress state is a function of a change in the fluid pressure field p_l:

$$d\sigma' = d\sigma + mdp_l \qquad (5)$$

where $d\sigma$ is the total stress increment and m is an identity tensor. The Perzyna viscoplastic model allows the modeling of the effects of the time rate in the plastic strain process. In a mechanical analysis, the resulting stresses and strains are time dependent, and a viscoplastic multiplier $\dot{\lambda}$ is applied to the plastic flow rule, as shown in (Equation 6):

$$\dot{\varepsilon}^{vp} = \frac{\langle\left(F\left(\sigma,h\right)\right)\rangle}{\eta} \frac{\partial F\left(\sigma,h\right)}{\partial \sigma} \qquad (6)$$

Therefore, the viscoplastic multiplier is a function of a penalty parameter $1/\eta$ and consider a monotonic function $\Phi(F(\sigma,h))$, and $\Phi(F(\sigma,h)) = 0 \Leftrightarrow F(\sigma,h) = 0$, where $F(\sigma,h)$ is the creep function and h are the internal variables for the plasticity model. Applying the flow rule (Equation 4) makes it possible to relate the state of stress with the strain via a viscoplastic constitutive tensor, D^{VP}. The creep function of the Mohr-Coulomb plasticity model is written in terms of the three stress invariants: p', J and θ, defined as the mean effective stress, deflection stress and Lode angle, respectively:

$$F\left(\sigma',h\right) = J - \left(\frac{c'}{tan\varphi'} + p'\right)G\left(\theta\right) = 0 \qquad (7)$$

where σ' is the effective stress, c' the effective cohesion and ϕ' is the effective friction angle.

2.2 Hydromechanical coupling

This work used a formulation that allows for coupling between changes in porosity and intrinsic permeability. The porosity variation is calculated using the solid equilibrium equation:

$$\frac{D\phi}{Dt} = \frac{\left(1-\phi\right)}{\rho^s} \frac{D\rho^s}{Dt} + \left(1-\phi\right)\dot{\varepsilon}_v \qquad (8)$$

where $\dot{\varepsilon}_v$ is the volumetric strain rate. The determination of permeability with the change in the rock strain is a complex function that depends on the elastic or inelastic regime of the material. The Mohr-Coulomb viscoplastic model uses a linear

law that relates the variation in permeability to the evolution of plastic shear strain, which is directly related to volumetric plastic strain at a given dilation angle (Guimarães et al., 2009).

3. Methodology

The simulation was carried out in a hypothetical bi-dimensional model describing a shallow reservoir cut by a fault. The simulation considered the oil reservoir production process, which involved operation of wells for injection and production of fluids. The fault zone was considered as a sealing region, a low permeability, geomechanical discontinuity within the reservoir. The fault is connected to a submarine slope over the reservoir, which was considered in equilibrium of stress. The model, described in Figure 1a, consists of a reservoir interval, a cap rock zone (overburden) with seal capacity, and an underlying interval (underburden). The sea level is 110 m above the overburden interval and the submarine slope (over the foot wall). The normal fault ends below the submarine slope which is formed by an overlying bed 130 m thick. The slope is located over the topographic displacement formed by the fault throw. The sea level depth over the hanging wall is −150 m, the base level of the submarine slope. The model is 1560 m wide, with a maximum thickness of 640 m in the slope region. The cap interval and underburden interval are both 270 m thick, and the reservoir interval is 80 m thick. The fault zone thickness is 10 m. The fault throw is 20 m (Figure 1).

The model was implemented as an unstructured finite element mesh of linear triangle elements (Figure 1b) with 8523 nodes and 16853 elements. The model contains 5 different materials which represent the slope, the reservoir interval, the cap interval and the overlying interval, and the fault zone. Each material is characterized by its mechanical and hydraulic properties—the modulus of elasticity E, cohesion c', and effective friction angle ϕ', porosity n, permeability k (materials were assumed to be isotropic), and Perzyna's viscous parameter $\eta / \Delta t$—summarized in Table 1.

The reservoir simulation involved two wells: an injector on the left side of the model, and a producer on the right side. The injector well is 155 m from the fault (left side) with a depth of 308 m, and the production well is located 20 m from the fault (right side), at a depth of 315 m. The bottomhole pressure (BHP) in the injector well is 4.2 MPa, above the reservoir pressure; at the production well, the pressure is 4.0 MPa, below the reservoir pressure. The mechanical and hydraulic boundary conditions are shown in Figure 2. The boundary conditions related to the movement restriction are applied horizontally, to limit lateral displacement, and vertically at the base of the model. Effective stress σ' is prescribed as zero at the surface of the seabed, the applied liquid pressure P_l corresponds to the equivalent to a water level P_w. The compressibility of the injection fluid and its density are 1.0×10^{-4} MPa^{-1} and 1001.7 kg/m^3, respectively. The simulation assumes a plane strain state.
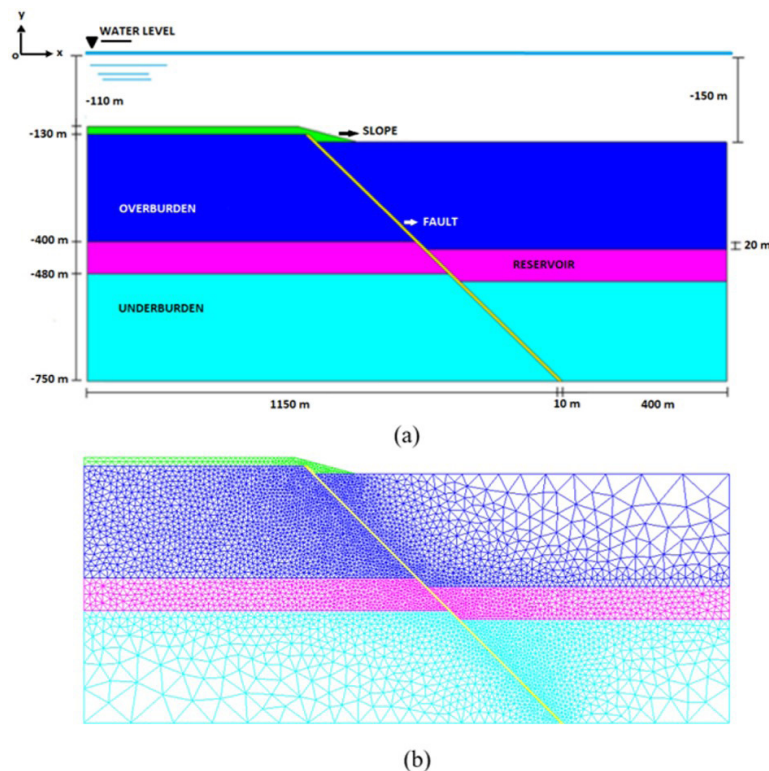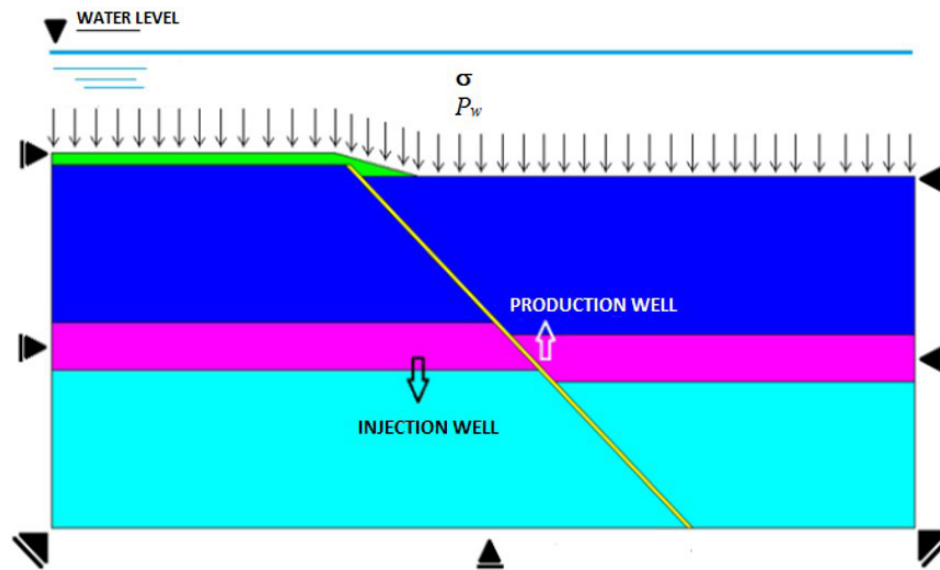

Figure 1. Details of the problem modeled: (a) geometries and materials; (b) FEM mesh.

Table 1. Property of materials.

Layer	E (MPa)	c' (MPa)	ϕ' (°)	k (m^2)	n	$\eta / \Delta t$
Slope	5	0,10	10	1x10^{-16}	0.48	10^4
Overburden	6780	2.30	26	1x10^{-25}	0.01	-
Underburden	10800	3.60	26	1x10^{-25}	0.01	-
Fault	8000	0.80	23	5x10^{-22}	0.1	10^4
Reservoir	15860	5.80	30	5x10^{-12}	0.2	-

Adapted from Pereira et al. (2014).

**Figure 2.** Initial and boundary conditions.

4. Results

The influence of the injection well was analyzed in the left region of the fault, close to the slope, observing the impact of the secondary oil recovery in the reservoir and the fault reactivation process.

The first variable to be considered is the pore pressure field, which changes due to well operation, leading to changes in the stress state variations inside the reservoir and for surrounding and cap rocks and geological structures. This can result in reactivating the fault structure through the shearing process, and increasing the permeability of damage zones and core fault, leading to fluid flow to the fault and increased pore pressure. Figure 3 shows the pore pressure distribution along the fault for an intermediate (Figure 3a) and final (Figure 3b) time step of the simulation process. The pressure increase inside the fault is evidence of reactivation and migration of the fluid.

Figure 4 shows the vectors indicating fluid flow from the reservoir through the fault. They reach the submarine slope base at top of field, indicating exudation at the seabed. These results show an important aspect to the slope stability process due to pressurizing the slope layer for a high pore pressure level.

The main fault reactivation indicators are the viscoplastic shear strain $\dot{\varepsilon}_d^{vp}$ (Figures 5a and b) and the consequent permeability fault increase (Figures 5c and d) as function of $\dot{\varepsilon}_d^{vp}$. The evolution of the shear plastic strain is a consequence of the stress path which reaches the Mohr-Coulomb yield surface, leading to a plastification process. Due the linear relation between the permeability changes and the shear plastic strain, as discussed in section 2.2, the fault permeability increases with plastification, opening the fault pores in a dilatancy process to fluid migration from the reservoir as explained above. This response has been widely observed, e.g. by Langhi et al. (2010) who realized a three-dimensional numerical simulation of the fault reactivation problem for a complex, sealed set of geological faults, accounting for hydro-mechanical coupling. This study considered shear strains and dilation as well as fluid flux as determining factors of fault leakage. Similar conclusions were presented in Guimarães et al. (2009, 2010), Rutqvist et al. (2007).

Pereira et al. (2014) presented a fault reactivation study for oil production scenario, applying methodology similar which was used in this study. They modeled a hydro-mechanical coupling and uncertainty analysis for fault properties, focusing on determining the maximum bottom hole pressure (BHP) without fault reactivation in which the plastic work (associated
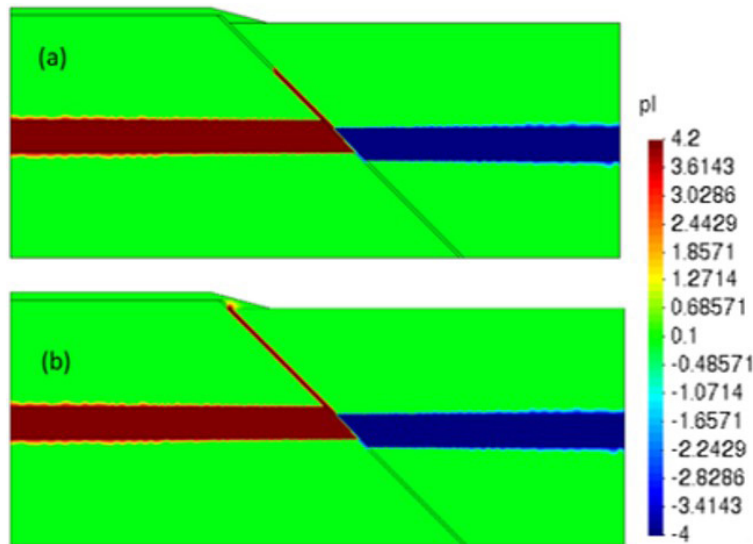
Figure 3. Pore pressure (MPa) at fault reactivation analysis: (a) pore pressure distribution at intermediary simulation time; (b) final distribution. Negative values indicate a drop in initial pore pressure, and positive values are related to increase because effective stress analysis.
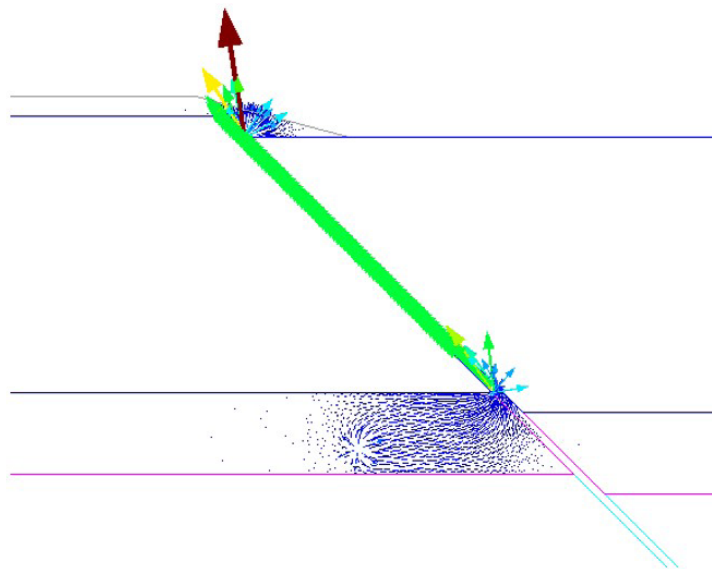

Figure 4. Distribution of fluid flow vectors to final time.

with shear plastic strain) and permeability increase, via the reactivation indicators as we describe in the present work. It is noteworthy that the permeability measure is in m^2 and is expressed on a negative log scale.

The pressurization of the fault structure during the reactivation process, associated with the change in the state of stress, causes differential displacements, especially at the top of the field where an expressive vertical displacement in the submarine slope is observed. This process occurs due to the ground uplift caused by the increased reservoir pore pressure as a function of well injector activity, which changes the initial stress state and pore pressure field. Then, the fluid injection in the compartmented reservoir causes volumetric expansion through hydro-mechanical coupling. Similar behavior has been presented as discussed by Khan et al. (2020), where the authors conducted a numerical investigation of CO_2 storage in reservoirs, analyzing the effects of pressure changes in the fault, reservoir, and surrounding rocks. The authors discussed the effects of reservoir size and boundary conditions on pore pressure buildup, on the ground uplift, and on fault reactivation and indicate the occurrence of fault reactivation and round uplift
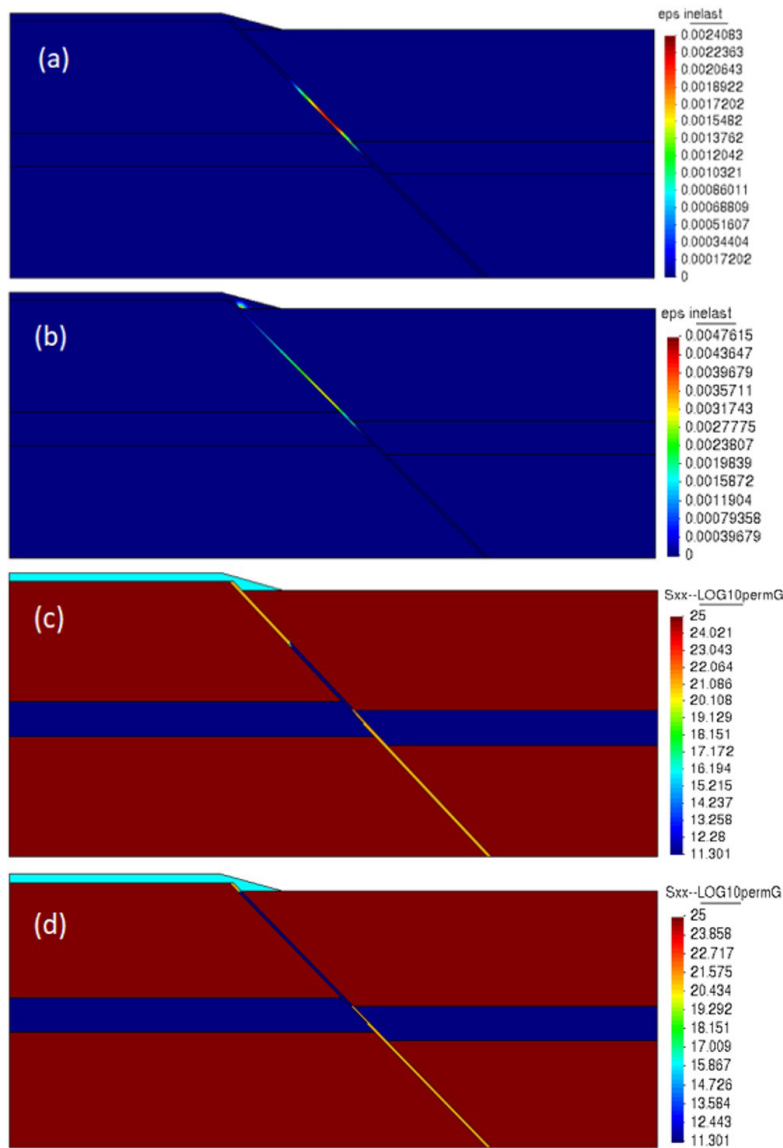
Figure 5. Fault reactivation indicators: (a) viscoplastic shear strain at intermediary simulation time; (b) final distribution of viscoplastic shear strain; (c) -log permeability change at intermediary simulation time; (d) final distribution of increased -log fault permeability.

associated with increased pore pressure of reservoir due to CO_2 injection. Then, the same hydro-mechanical behavior is observed as in the present work.

These aspects can be observed in Figures 6a and 6b that show the final distribution of vertical and horizontal displacements of the field. The figures show a greater positive displacement on the slope; in the region where the fault meets, a dilatation process occurs due to the injection of the fluid, as shown in Figure 6. For horizontal displacements, it is possible to identify a discontinuous displacement field in the surrounding rocks for two sides of the fault, showing the shearing effect of the structure.

Following the above general analysis of the oilfield and geological fault, showing the reactivation process discussions, the mechanical analysis of the submarine slope is now carried out, analyzing the consequences of reservoir pressurization and fault reactivation effects.

Initially, is intended aim to analyze the pore pressure increase, shear stress and shear plastic strain occurrence in the slope layer as a function of the fault reactivation that led to fluid flow from the reservoir to the base of slope as observed in Figure 7. The slope shearing follows the top of the fault movement and presents irreversible (plastic) strains (Figure 7b), indicating loss of shear strength and susceptibility to failure. Increasing the pore pressure (Figure 7a) to a high level to inject fluid pressure in the reservoir promotes an expressive unstable condition of the soil, conducive to slope movement. Additional evidence of slope failure is the pattern and level of shear stress band localized at the slope, showing a failure surface (Figure 7c).
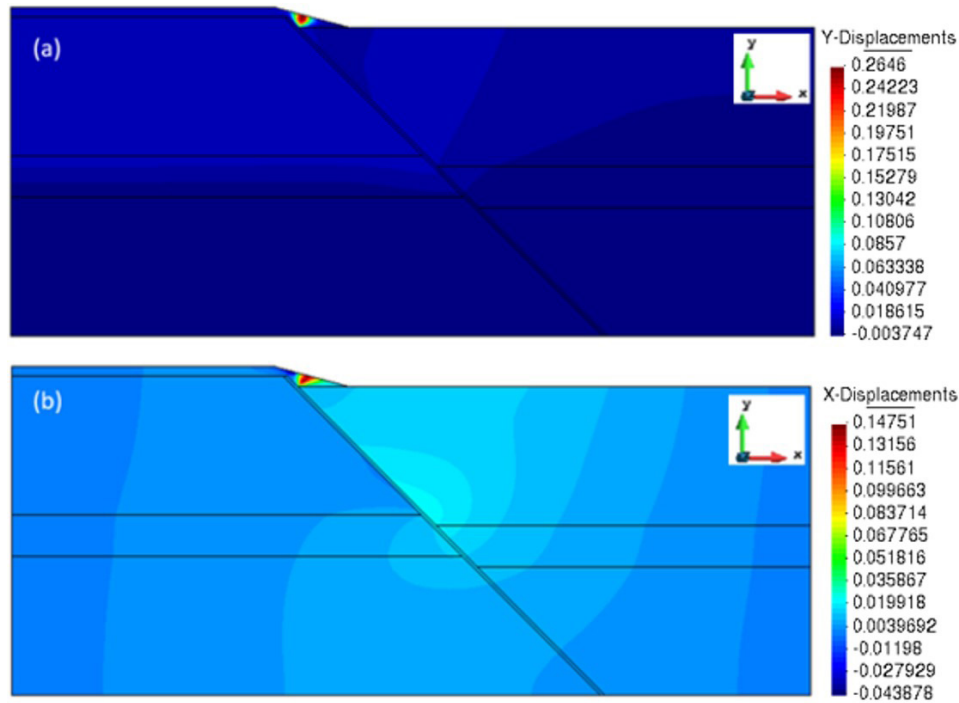
Figure 6. Final distribution of displacements: (a) vertical displacements; (b) horizontal displacements.
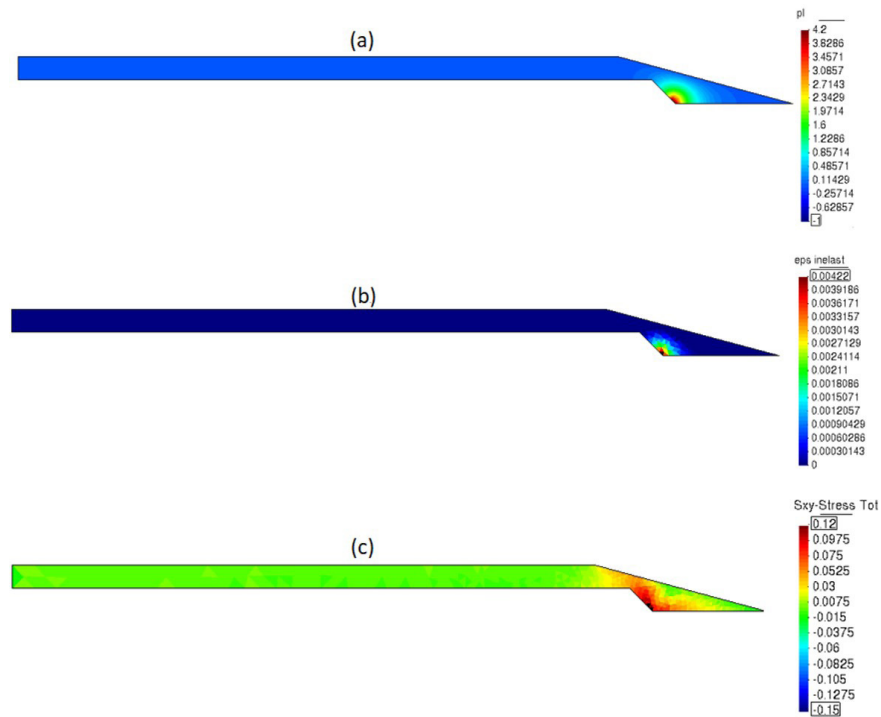
Figure 7. Submarine slope analysis – final distribution: (a) pore pressure (MPa); (b) shear plastic; (c) shear strain stress (MPa).

The evolution of shear plastic strain and pore pressure for a selected point can be observed in Figure 8. Focusing on this point makes it possible to identify the evolution of pore pressure with the soil plastification and the stabilization of pore pressure under expressive increase of shear plastic strain indicating two failures, possibly associated with fault movement history. The stabilization of pore pressure for these instants can be associated with the sudden increase in

permeability which leads to fast fluid percolation reaching the pore pressure value.

The slope soil presents an initial and low permeability, and it shows an expressive and faster increase as shown in Figure 9. The permeability measure considered is in m² and expressed logarithmically, and the reduction of *y*-axis values is related to the exponent, indicating an increase in 3 orders of magnitude.

After a time, the shearing process in a dilatant behavior continues and the permeability is increased gradually followed by an increase in pore pressure. Similar behavior is observed in an analysis of dilatant response through the analysis of permeability and porosity evolution as shown in Figure 9. It is possible to observe a few increases of porosity with change in permeability indicating a volumetric inelastic strain. The curve contours are like the response observed in
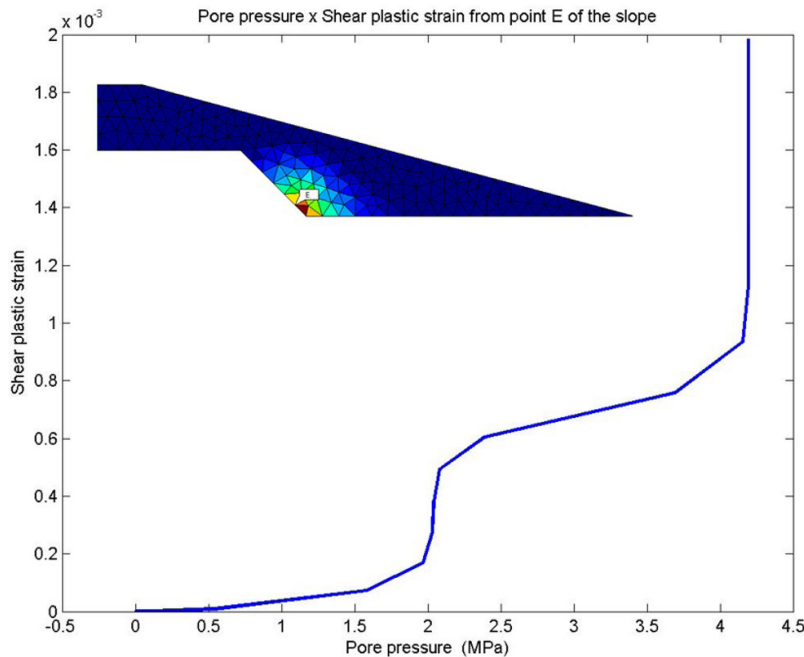
Figure 8. Submarine slope analysis – shear plastic strain vs pore pressure (MPa) at point E (contact between slope layer and fault).
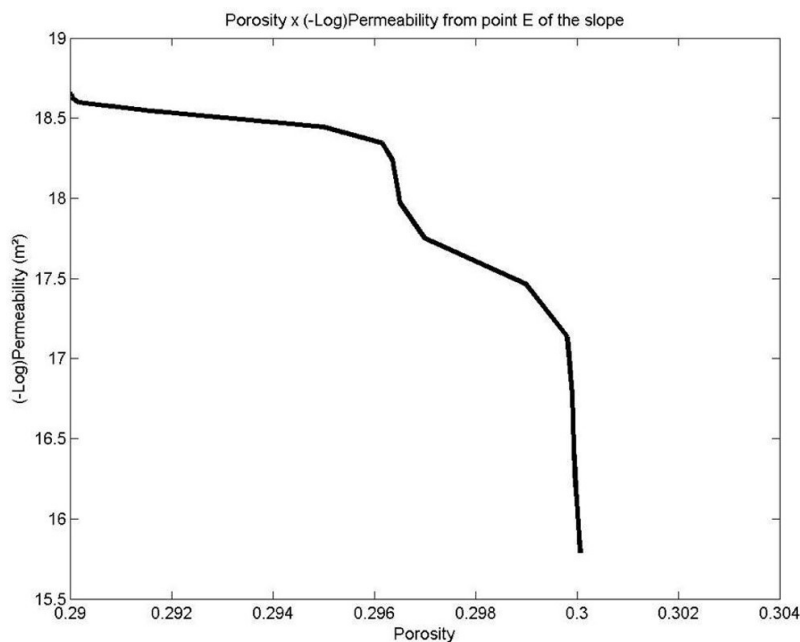

Figure 9. Submarine slope analysis: -log of permeability (m²) vs porosity at point E (contact between slope layer and fault).

the relation between shear plastic strain and pore pressure (Figure 8).

Both horizontal and vertical displacement occurred on the slope, as shown in Figures 10a and 10b, respectively. The horizontal displacement where the fault touches the slope was approximately 14 cm. There was a displacement in expansive subsidence (ground uplift) of about 26 cm, pushing the slope laterally, therefore, the instability is caused by pressurization and plastic strain in the slope.

Finally, to investigate the relationship between the slope displacements and the development of fault reactivation, two mesh elements were selected at different regions on the slope layer, and the evolution of displacements over time was evaluated (Figure 11), associating them with the evolution

of shear plastic strains mapped at points on the geological fault (Figure 12). It is verified that the displacements at the different points of the slope occur from the process of fault reactivation, indicating a progressive movement of the slope in the downstream direction. A greater intensification of the reactivation process is observed by the increase of plastic strains, between 9 and 10 days. This process causes a change in the pattern of slope displacements, with an increasing trend at point A (foot of the slope), and with an inflection point at the top node of the slope, point B, for a negative displacement associated with the shearing process and ground uplift at the top of the fault. A time-dependent behavior of the soft clay of the slope is verified, indicating an adequate application of the viscoplastic model.
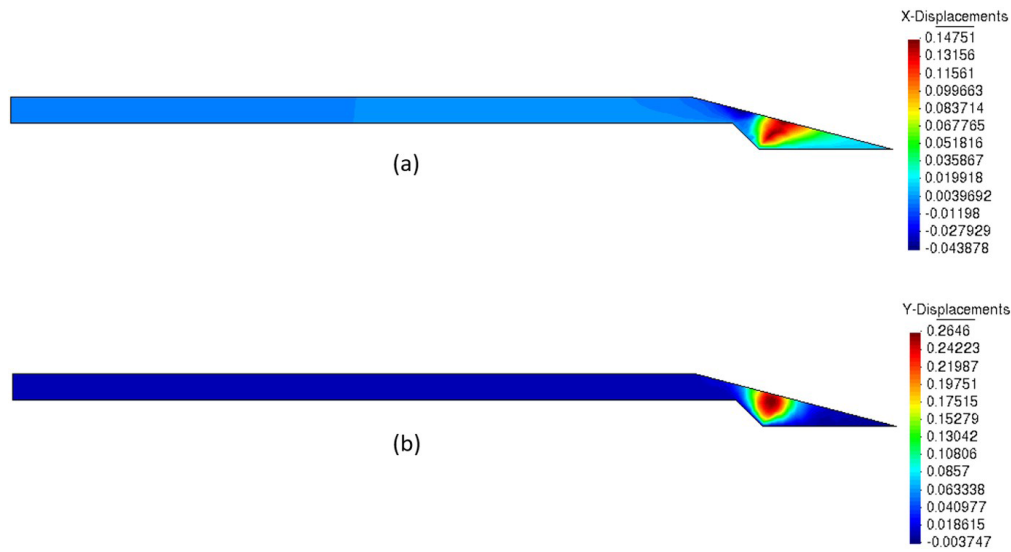
Figure 10. Submarine slope analysis – final distribution: (a) horizontal displacements (m); (b) vertical displacements (m).
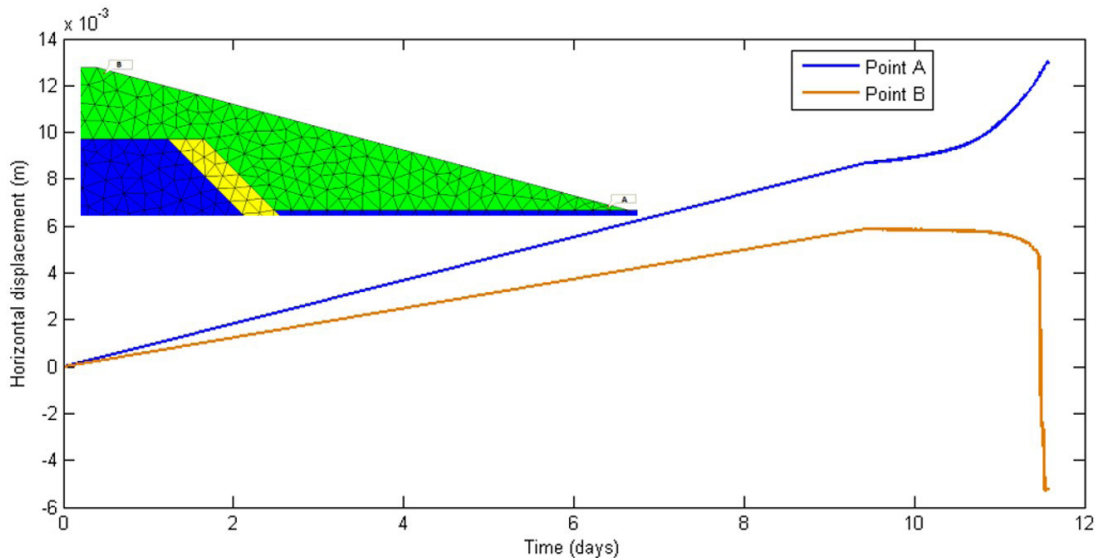
Figure 11. Submarine slope analysis – horizontal displacements (m) evolution of two analysis points: base and top of submarine slope.
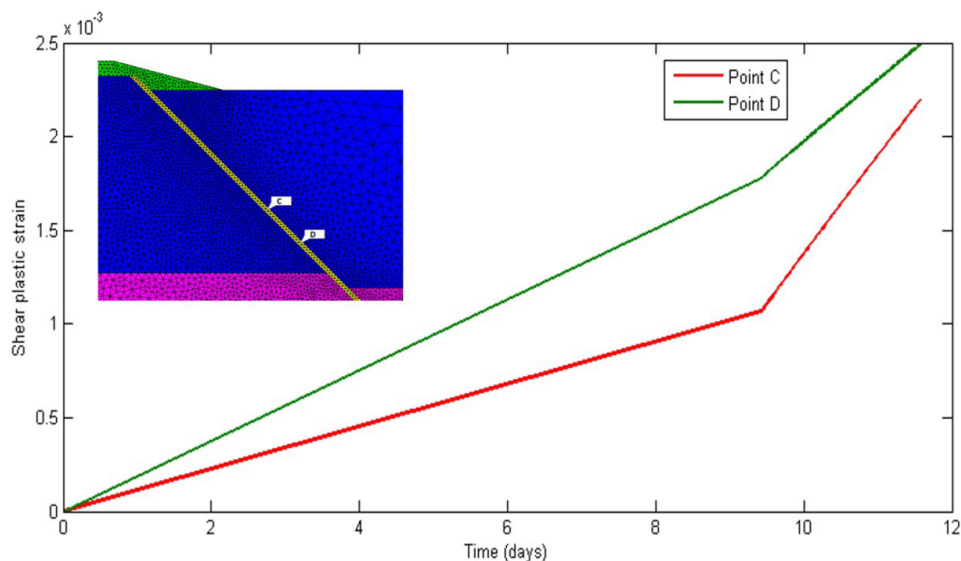
Figure 12. Analysis of the shear plastic strain at two different fault points analysis.

5. Discussion

Adopting shear plastic strain for slope stability analysis and the evolution of shear stress localization were previously discussed in studies like Dey et al. (2016), where a slope stability problem was modeled for large strain using a finite element approach analysis to study shear plastic strain localization and associated displacements. The authors comment that a finite element analysis performs well because initiation and progressive evolution of the weak shear zones in the submarine slopes cannot be simulated by the limit equilibrium method. They also observe, importantly, the relation between decreased shear strength in the initiated failure zone and factors such as geological activities, pore pressure increase, earthquake, and plastic shear deformation. The results obtained by the present study showed similar relations between the effects that trigger the instability and the conditions which led to the slope failure.

Numerical analysis by Zhang & Puzrin (2022), demonstrated how an initial failure surface evolves to a large submarine landslide, and they quantified the different phases. For these authors, the failure zone formation for submarine slope is associated with loss of soil strength due to shearing (shear stress development) and because the pore pressure increases, which is similar to the effects described in this study. Urgeles & Camerlenghi (2013), compiled a catalog of submarine slope failure events in the Mediterranean Sea, and discussed the trigger mechanisms and relationship with fluid flow. They indicate that, amongst various factors, the increase in shear stress on the slope is the most common cause of failure.

Shan et al. (2022) discusses how earthquake, high sedimentation rate and diapirism are the most common triggers for submarine slope stability, suggesting more analyses that account for the hydro-mechanical coupling and consider seismicity, pore pressure changes and water turbidity as warning factors for slope stability risk. In the present study, we indicate that the fault reactivation led to increased pore pressure in the submarine slope, and we consider this result as a trigger factor by which fault reactivation can lead to seismicity. Rutqvist et al. (2013) studied potential fault reactivation due to fluid injection in a hydraulic fracturing operation and the associated induced seismicity. The authors showed that the fault reactivation presents a relation with micro-seismic events and, when faults are present in the field, it is possible that the occurrence of large seismic events depends on factors such as initial fault permeability, in situ stress state, and shear strength properties of faults.

6. Conclusions

For the scenario analyzed, subject to a few simplifications in geometries and the homogeneity of the geological fault and submarine slope properties, the work showed a clear influence of the oil production process on the mechanical behavior of the submarine slope, due to fault reactivation. The reservoir pressure variation was the trigger for fault reactivation, and the overlying submarine slope. This was evidenced by through the development of shear plastic strains, permeability change, shear stress and pore pressure increase for fault and slope materials as well as by the displacement observed in the slope. This stress-strain response is relevant because displacement reached up to 26 cm, which should be contextualized by the fact that the slope is also under water pressure.

The pore pressure increase is directly associated with the increase in the soil and rock permeability, as a function of shear plastic strain. A numerical simulation with hydro-mechanical coupling is an adequate way to analyze this kind of problem. Furthermore, it is suggested using different types of constitutive models for the evaluation of the submarine slope stability.

The methodology used in this work can be applied to real oil reservoir problems, given adequate information about submarine slope geometries and important attributes such as declivity and seabed relief.

It is of great importance to investigate the impact of oil and gas production in faulted reservoirs, considering the need to assess the risk of reactivation and its effect on the stability of submarine slopes with implications for environmental and economic damage, since slope instability can lead to damage to pipelines, and offshore wind towers, and catastrophic hydrocarbon leakage.

It is suggested that a geomechanical analysis to predict reactivation risks is highly necessary because it can define the safe levels of fluid injection pressure for operating reservoirs that present faults connected to shallow regions of the sedimentary column and submarine slopes.

Additionally, submarine landslides can occur due to post-failure slope conditions, remobilizing and displacing large volumes of sediments. This type of simulation needs a large-strain analysis, different from the approach presented here, where the interest was the pre-failure and failure occurrence caused by fault reactivation as the triggering mechanism.

Acknowledgements

Declaration of interest

The authors have no conflicts of interest to declare. All co-authors have observed and affirmed the contents of the paper and there is no financial interest to report.

Authors' contributions

Tasso Carvalho da Silva: conceptualization, methodology, data analysis, writing – original draft. Igor Fernandes Gomes: conceptualization, methodology, data analysis, writing – original draft, supervision, review & editing, funding acquisition. Tiago Siqueira de Miranda: conceptualization, review & editing. Julliana de Paiva Valadares Fernandes: writing – review & editing. José Antônio Barbosa: conceptualization, review & editing. Leonardo José do Nascimento Guimarães: review & editing, funding acquisition.

Data availability

The datasets generated analyzed in the course of the current study are available from the corresponding author upon request.

List of symbols

b	volumetric vector of body forces
c'	effective cohesion
f_l	fluid phase source/sink mass term
g	gravity vector
h	hardening parameter
k	permeability
m	identity tensor
n	porosity
p'	effective mean stress
p_l	fluid pressure
q_l	Darcy flow vector
$\dot{u}$	nodal displacement
D^E	elastic constitutive tensor
D^{VP}	viscoplastic constitutive tensor
E	Young's modulus
F	fluency function
J	deviator stress
K	permeability tensor
$\dot{\varepsilon}^{vp}$	viscoplastic strain rate
$\dot{\varepsilon}_v$	volumetric strain rate
ε	total strain
ε^E	elastic strain
ε^{VP}	viscoplastic strain
$\dot{\varepsilon}_d^{vp}$	viscoplastic shear strain
∇	divergent operator
η	Perzyna's viscous regularization parameter
θ	Lode's Angle
$\dot{\lambda}$	viscoplastic multiplier
μ_l	fluid phase viscosity
ρ_l	fluid phase density
ρ^s	solid phase density
σ	stress tensor
σ'	effective stress tensor
ϕ	rock porosity
ϕ'	effective friction angle

References

Bakhsh, T.T., Simpson, K., & Lapierre, T. (2021). Potential geo-hazard to floating offshore wind farms in the US pacific. In *Proceedings of the ASME 2021 3rd International Offshore Wind Technical Conference (IOWTC 2021)*. New York: American Society of Mechanical Engineers.

Billi, A., Salvini, F., & Storti, F. (2003). The damage zone-fault core transition in carbonate rocks: implications for fault growth, structure, and permeability. *Journal of*

Structural Geology, 25(11), 1779-1794. http://dx.doi.org/10.1016/S0191-8141(03)00037-3.

Caine, J.S., Evans, J.P., & Forster, C.B. (1996). Fault zone architecture and permeability structure. *Geology*, 24(11), 1025-1028. http://dx.doi.org/10.1130/0091-7613(1996)024<1025:FZAAPS>2.3.CO;2.

Cappa, F., & Rutqvist, J. (2011). Modeling of coupled deformation and permeability evolution during fault reactivation induced by deep underground injection of CO_2. *International Journal of Greenhouse Gas Control*, 5(2), 336-346. http://dx.doi.org/10.1016/j.ijggc.2010.08.005.

Celestino, M.A., Miranda, T.S., Mariano, G., Alencar, M.L., Carvalho, B.R.B.M., Falcão, T.C., Topan, J.G., Barbosa, J.A., & Gomes, I.F. (2020). Fault damage zones width: implications for the tectonic evolution of the northern border of the Araripe Basin, Brazil, NE Brazil. *Journal of Structural Geology*, 138, 104116. http://dx.doi.org/10.1016/j.jsg.2020.104116.

Choi, J.H., Edwards, P., Ko, K., & Kim, Y.S. (2016). Definition and classification of fault damage zones: a review and a new methodological approach. *Earth-Science Reviews*, 152, 70-87. http://dx.doi.org/10.1016/j.earscirev.2015.11.006.

Dey, R., Hawlader, B.C., Phillips, R., & Soga, K. (2016). Numerical modelling of submarine landslides with sensitive clay layers. *Geotechnique*, 66(6), 454-468. http://dx.doi.org/10.1680/jgeot.15.P.111.

Fossen, H. (2016). *Structural geology* (2nd ed., 524 p.). Cambridge: Cambridge University Press.

Gudmundsson, A. (2004). Effects of Young's modulus on fault displacement. *Comptes Rendus Geoscience*, 336(1), 85-92. http://dx.doi.org/10.1016/j.crte.2003.09.018.

Gue, C.S. (2012). *Submarine landslide flows simulation through centrifuge modeling* [Doctoral thesis]. University of Cambridge, Cambridge.

Guimarães, L.J.N., Gens, A., & Olivella, S. (2007). Coupled thermo-hydro-mechanical and chemical analysis of expansive clay subjected to heating and hydration. *Transport in Porous Media*, 66(3), 341-372. http://dx.doi.org/10.1007/s11242-006-0014-z.

Guimarães, L.J.N., Gomes, I.F., & Fernandes, J.P.V. (2009). Influence of mechanical constitutive model on the coupled hydro-geomechanical analysis of fault reactivation. In *Proceedings of the SPE Reservoir Simulation Symposium* (SPE-119168-MS), The Woodlands, Texas, USA.

Guimarães, L.J.N., Gomes, I.F., Barbosa, J.A., & Almeida, R.P.M. (2010). Numerical modelling of CO2 flow through deformable aquifers with the possibility of fault reactivation. In *Proceedings of the 6th International Congress on Environmental Geotechnics*, New Delhi, India.

Katz, O., Reuven, E., & Aharonov, E. (2015). Submarine landslides and fault scarps along the eastern Mediterranean Israeli continental-slope. *Marine Geology*, 369, 100-115. http://dx.doi.org/10.1016/j.margeo.2015.08.006

Khan, S., Khulief, Y.A., & Al-Shuhail, A.A. (2020). Effects of reservoir size and boundary conditions on pore-pressure buildup and fault reactivation during CO_2 injection in deep geological reservoirs. *Environmental Earth Sciences*, 79(12), 294. http://dx.doi.org/10.1007/s12665-020-09040-0.

Langhi, L., Zhang, Y., Gartrell, A., Underschultz, J., & Dewhurst, D. (2010). Evaluating hydrocarbon trap integrity during fault reactivation using geomechanical three-dimensional modeling: an example from the Timor Sea, Australia. *AAPG Bulletin*, 94(4), 567-591. http://dx.doi.org/10.1306/10130909046.

Leynaud, D., Mienert, J., & Nadim, F. (2004). Slope stability assessment of the Helland Hansen area offshore the mid-Norwegian margin. *Marine Geology*, 213(1–4), 457-480. http://dx.doi.org/10.1016/j.margeo.2004.10.019.

Ma, G., Kirby, J.T., & Shi, F. (2013). Numerical simulation of tsunami waves generated by deformable submarine landslides. *Ocean Modelling*, 69, 146-165. http://dx.doi.org/10.1016/j.ocemod.2013.07.001.

Masson, D.G., Wynn, R.B., & Talling, P.J. (2010). Large landslides on passive continental margins: processes, hypotheses, and outstanding questions. In D.C. Mosher, R.C. Shipp, L. Moscardelli, J.D. Chaytor, C.D.P. Baxter, H.J. Lee & R. Urgeles (Eds.), *Submarine mass movements and their consequences* (pp. 153-165). Cham: Springer.

Matsumoto, N., & Shigematsu, N. (2018). In-situ permeability of fault zones estimated by hydraulic tests and continuous ground water-pressure observations Earth. *Earth, Planets, and Space*, 70(1), 13. http://dx.doi.org/10.1186/s40623-017-0765-5.

Mitchell, T.M., & Faulkner, D.R. (2009). The nature and origin of off-fault damage surrounding strike-slip fault zones with a wide range of displacements: A field study from the Atacama fault system, northern Chile. *Journal of Structural Geology*, 31(8), 802-816. http://dx.doi.org/10.1016/j.jsg.2009.05.002.

Myers, R.D. (1999). *Structure and hydraulics of brittle faults in sandstone* [Doctoral thesis]. Stanford University, Stanford, CA.

Olivella, S., Carrera, J., Gens, A., & Alonso, E.E. (1995). Numerical formulation for a Simulator (CODE_BRIGHT) for the coupled analysis of saline media. *Engineering Computations*, 7, 87-112.

Peacock, D.C.P., Dimmen, V., Rotevatn, A., & Sanderson, D.J. (2017). A broader classification of damage zones. *Journal of Structural Geology*, 102, 179-192. http://dx.doi.org/10.1016/j.jsg.2017.08.004.

Pereira, L.C., Guimarães, L.J.N., Horowitz, B., & Sánchez, M. (2014). Coupled hydro-mechanical fault reactivation analysis incorporating evidence theory for uncertainty quantification. *Computers and Geotechnics*, 56, 202-215. http://dx.doi.org/10.1016/j.compgeo.2013.12.007.

Perzyna, P. (1966). Fundamental problems in viscoplasticity. *Advances in Applied Mechanics*, 9, 243-377. http://dx.doi.org/10.1016/S0065-2156(08)70009-7.

Puzrin, A.M., Gray, T.E., & Hill, A.J. (2015). Significance of the actual nonlinear slope geometry for catastrophic failure in submarine landslides. *Proceedings - Royal Society. Mathematical, Physical and Engineering Sciences*, 471(2175), 20140772. http://dx.doi.org/10.1098/rspa.2014.0772.

Quevedo, R., Ramirez, M., & Roehl, D. (2017). 2D and 3D numerical modeling of fault reactivation. In *Proceedings of the 51st U.S. Rock Mechanics/Geomechanics Symposium*, San Francisco, CA, USA.

Quinn, P.E., Diederichs, M.S., Rowe, R.K., & Hutchinson, D.J. (2011). A new model for large landslides in sensitive clay using a fracture mechanics approach. *Canadian Geotechnical Journal*, 48(8), 1151-1162. http://dx.doi.org/10.1139/t11-025.

Quinn, P.E., Diederichs, M.S., Rowe, R.K., & Hutchinson, D.J. (2012). Development of progressive failure in sensitive clay slopes. *Canadian Geotechnical Journal*, 49(7), 782-795. http://dx.doi.org/10.1139/t2012-034.

Rutqvist, J., Birkholzer, J., Cappa, F., & Tsang, C.F. (2007). Estimating maximum sustainable injection pressure during geological sequestration of CO_2 using coupled fluid flow and geomechanical fault-slip analysis. *Energy Conversion and Management*, 48(6), 1798-1807. http://dx.doi.org/10.1016/j.enconman.2007.01.021.

Rutqvist, J., Rinaldi, A.P., Cappa, F., & Moridis, G.J. (2013). Modeling of fault reactivation and induced seismicity during hydraulic fracturing of shale-gas reservoirs. *Journal of Petroleum Science Engineering*, 107, 31-44. http://dx.doi.org/10.1016/j.petrol.2013.04.023.

Scarselli, N. (2020). Chapter 16 - Submarine landslides – architecture, controlling factors and environments: a summary. In N. Scarselli, J. Adam, D. Chiarella, D.G. Roberts & A.W. Bally (Eds.), *Regional geology and tectonics* (2nd ed., pp. 417-439). Amsterdam: Elsevier.

Scarselli, N., McClay, K., & Elders, C. (2016). Seismic geomorphology of cretaceous megaslides offshore Namibia (Orange Basin): insights into segmentation and degradation of gravity-driven linked systems. *Marine and Petroleum Geology*, 75, 151-180. http://dx.doi.org/10.1016/j.marpetgeo.2016.03.012.

Shan, Z., Wu, H., Ni, W., Sun, M., Wang, K., Zhao, L., Lou, Y., Liu, A., Xie, W., Zheng, X., & Guo, X. (2022). Recent technological and methodological advances for the investigation of submarine landslides. *Journal of Marine Science and Engineering*, 10(11), 1728. http://dx.doi.org/10.3390/jmse10111728.

Silva, J.P., Gomes, I.F., Santos, R.F.V.C., Miranda, T.S., Guedes, R.P., Barbosa, J.A., Guimarães, E.X., Beserra, L.B., & Guimarães, L.J.N. (2021). Topological analysis of fracture networks integrated with flow simulation models for equivalente fracture permeability estimation. *Journal of Structural Geology*, 147, 104338.

Simo, J.C., & Hughes, T.J.R. (1998). Integration algorithms for plasticity and viscoplasticity. In J.C. Simo & T.J.R. Hughes (Eds.), *Computational Inelasticity* (pp. 113-151). New York: Springer.

Soltanzadeh, H., & Hawkes, C.D. (2008). Semi-analytical models for stress change and fault reactivation induced by reservoir production and injection. *Journal of Petroleum Science Engineering*, 60(2), 71-85. http://dx.doi.org/10.1016/j.petrol.2007.05.006.

Souza, F.M., Gomes, I.F., Nogueira, F.C.C., Vasconcelos, D.L., Canabarro, B.M., Souza, J.A.B., Guimarães, L.J.N., & Beserra, L.B.S. (2022). 2D modeling and simulation of deformation bands' effect on fluid flow: implications for hydraulic properties in siliciclastic reservoirs. *Journal of Structural Geology*, 158, 104581. http://dx.doi.org/10.1016/j.jsg.2022.104581.

Stoecklin, A., Trapper, P., & Puzrin, A.M. (2021). Controlling factors for post-failure evolution of subaqueous landslides. *Geotechnique*, 71(10), 879-892. http://dx.doi.org/10.1680/jgeot.19.P.230.

ten Brink, U.S.T., Lee, H.J., Geist, E.L., & Twichell, D. (2009). Assessment of tsunami hazard to the U.S. East Coast using relationships between submarine landslides and earthquakes. *Marine Geology*, 264(1-2), 65-73. http://dx.doi.org/10.1016/j.margeo.2008.05.011.

Torabi, A., Ellingsen, T.S.S., Johannessen, M.U., Alaei, B., Rotevatn, A., & Chiarella, D. (2020). *Fault zone architecture and its scaling laws: where does the damage zone start and stop?* (Special Publications Series, No. 496, pp. 99-124). London: Geological Society. http://dx.doi.org/10.1144/SP496-2018-151.

Urgeles, R., & Camerlenghi, A. (2013). Submarine landslides of the Mediterranean Sea: trigger mechanisms, dynamics, and frequency-magnitude distribution. *Journal of Geophysical Research. Earth Surface*, 118(4), 2600-2618. http://dx.doi.org/10.1002/2013JF002720.

Yang, P., Guanghui, W., Perach, N., Ai Duc, N., Yongquan, C., Shuai, Y., Yue-xing, F., Zhanli, R., & Jian, Z. (2021). In situ LA-ICPMS UPb dating and geochemical characterization of fault-zone calcite in the central Tarim Basin, northwest China: implications for fluid circulation and fault reactivation. *Chemical Geology*, 568, 120125. http://dx.doi.org/10.1016/j.chemgeo.2021.120125.

Yincan, Y. (2017). Submarine landslides. In Y. Yincan (Ed.), *Marine geo-hazards in China* (chap. 6, pp. 179-267). Amsterdam: Elsevier.

Zhang, W., & Puzrin, A.M. (2022). How small slip surfaces evolve into large submarine landslides—insight from 3D numerical modeling. *Journal of Geophysical Research: Earth Surface*, 127(7), e2022JF006640. https://doi.org/10.1029/2022JF006640.

Zhang, Y., Wang, Z., Yang, Q., & Wang, H. (2019). Numerical analysis of the impact forces exerted by submarine landslides on pipelines. *Applied Ocean Research*, 92, 101936. http://dx.doi.org/10.1016/j.apor.2019.101936.

14

Silva et al., Soil. Rocks, São Paulo, 2023 46(4):e2023006523